UNIVERSITY OF CAMBRIDGE

ARCHAEOLOGY OF THE MILKY WAY:

CONCERNING A BAR, A BULGE AND A CLOUD

IULIA TEODORA SIMION

INSTITUTE OF ASTRONOMY

& WOLFSON COLLEGE

SUPERVISOR:

DR. VASILY BELOKUROV

CO - SUPERVISORS:

DR. MIKE IRWIN and DR. SERGEY KOPOSOV

This dissertation is submitted for the degree of Doctor of Philosophy

December 2015

DECLARATION OF ORIGINALITY

I, Iulia Teodora Simion, declare that this thesis titled, 'Archeology of the Milky Way' and the work presented in it are my own. I confirm that:

- This work was done wholly while in candidature for the degree of Doctor of Philosophy at the University of Cambridge. This thesis has not previously been submitted for a degree or any other qualification at this University or any other institution.
- With the exception of quotations or figures who are credited to others, this thesis is entirely my own work. Where I have consulted the published work of others, this is always clearly attributed. When the outcome of work done in collaboration with others is included, this specifically indicated in the text. The first, introductory Chapter mainly draws on the work of others.
- Chapter 2 was published as *Strong RR Lyrae excess in the Hercules-Aquila Cloud*, I. Simion, V. Belokurov, M. Irwin, S. Koposov 2014, MNRAS, 411, 161 .
- The length of this thesis does not exceed the stated limit of the Degree Committee of Physics and Chemistry of 60,000 words.

Signed

Date

Contents

List of Figures

List of Tables

1

Spectroscopic follow-up of the HAC RR Lyrae. Disentangling the inner halo debris

1.1 Introduction: the HAC spectroscopic follow-up

The Hercules-Aquila Cloud is a stellar cloud extending over a large area of the sky detected as a prominent overdensity of RRab in the Galactic Southern Hemisphere at heliocentric distances between 12 and 25 kpc (e.g. Fig. **??**). Given its position in the inner Milky Way and the strong presence of an old metal poor RR Lyrae population, the Hercules Aquila Cloud is probably related to an accretion event more than 8 Gyrs old that occurred when our Galaxy was experiencing rapid growth. Nonetheless, theory and simulations Helmi et al. (1999) predict that even many Gyr after infall, debris should show characteristic signatures of an accreted galaxy in velocity space. In fact, kinematic data is incredibly useful for identifying substructures (e.g. the Pisces Overdensity), discerning between the nature of progenitors (globular clusters versus dwarf spheroidal galaxies) and constraining the orbits of the debris (Casetti-Dinescu et al. 2009, Virgo Overdensity). Compared to other tracers (e.g. main sequence turn off stars or blue stragglers) the RRab Lyrae have the advantage of being bright stars ($M_V = 0.6$ at $[Fe/H] = -1.5$ dex) that can be detected at large distances. They are also standard candles with $\sim 7\%$ uncertainty in distance

for the CSS data and, thanks to their characteristic saw-tooth-shaped light curve (see Fig. 1.8), they are easy to be separated from contaminants (RRc or binary systems). We designed a follow-up program to measure radial velocities of RRab in the Hercules-Aquila Cloud excess discovered by Simion et al. 2014 (the content of the previous chapter) in the Catalina Schmidt Survey.

The sample of 225 HAC RRab candidates (all circles in Fig. 1.1) is selected from the CSS catalogue (black dots in the same figure) with $28^\circ < l < 55^\circ$, $-45^\circ < b < -20^\circ$ and $15 < D/kpc < 20$: this is the region where the RR Lyrae overdensity is most prominent and we expect that up to 25% of the sample to belong to the cloud. The targets are named 'HAC1' to 'HAC225', ordered according to increasing right ascension.

The observations were taken using the ModSpec spectrograph on the 2.4m Hiltner telescope at the MDM observatory on Kitt Peak during six nights (labeled 'n1' to 'n6' in Table 1.3) between the 29th of August 2014 and the 3rd of September 2014. On the third night ('n3') the instrument had a technical problem and on the last night ('n6') the weather was bad so we only observed a few targets in those nights. In total we obtained 59 observations (blue circles in Fig. 1.1), each with at least one exposure. The spectrograph configuration used a 600 groove mm^{-1} grating with central wavelength at 5300 $\mathring{A}$and the detector was a 2048x2048 CCD with 15 micron pixels (Echelle). The wavelength coverage of the spectrograph was about 3500 $\mathring{A}$ and included the H_γ, H_β, H_α Balmer lines (at 4341, 4861, 6563 $\mathring{A}$) and two [OI] sky lines (at 5577 and 6300 $\mathring{A}$), useful for checking for offsets in the radial velocity determination. The instrument was set up for a resolution of 2 $\mathring{A}$, and it should allow us to get radial velocities accurate to 10 km/s. The range of magnitudes desired to probe distances of $15 < D/kpc < 20$ is $16.5 < V_0 < 17.1$. To achieve a S/N of 20 per pixel with this instrument set-up, an integration time of 750 seconds was needed for targets with $V_0 = 16.5$ mag. To limit the integration time we only observed targets brighter than $V < 17.5$ mag, which means observing preferentially closer targets. In practice, we used integration times of 600 and 900 seconds, depending on the seeing, airmass and brightness.

To determine the wavelength solution, Neon, Xenon, Argon and Mercury comparison lamp spectra were taken throughout the night, specifically after long telescope slews to account for telescope flexure. In addition, arc lamps, flat field and bias frames were obtained at the beginning of each night.

1.2 Data reduction: basic processing steps

The data reduction is done using a collection of *IRAF* and *Python* routines. The following subsections describe the outline of the reductions steps. All these procedures are applied to the observations of each

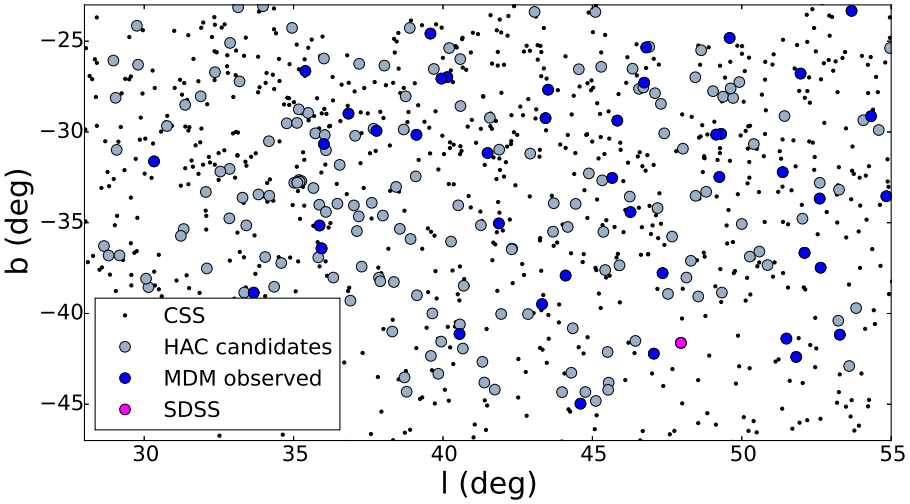

Figure 1.1: RR Lyrae from the CSS survey in Galactic coordinates in the southern Hercules Aquila Cloud. Full blue circles are the clean sample of observed targets, black dots are all CSS stars that are outside our selection for the HAC: $28^\circ < l < 55^\circ$, $-45^\circ < b < -20^\circ$, V <17.5 mag and $15 < D/kpc < 20$. All stars that pass the selection are shown with full circles (gray corresponds to the targets that have not been observed and blue to the targets that were observed). The pink full circle is a CSS HAC candidate with v_{GSR} obtained from SDSS.

night separately.

1.2.1 Calibration bias frame

A region of the frame (labeled 'overscan' in Fig. 1.3) is dedicated to measuring the amplifier bias level, or the 'zero' level that needs to be subtracted from the data. We use the IRAF *ccdproc* task to determine the average offset level ("OS") and subtract it from all the pixels in the data frame.

The "bias frames" are zero exposure time frames with the shutter closed designed to measure the bias generated during the read out of the CCD. To increase the S/N at such low counts we take the median of several frames (10 at the beginning and 10 at the end of each night, $N_b = 20$) to obtain a "calibration bias frame". We subtract from all images the master bias and, from each individual frame, the overscan (OS) level.

1.2.2 Calibration flat field frame

A flat-field frame is needed to correct for the pixel-to-pixel sensitivity variations in the detector (and the small-scale variations in the throughput of the instrument optics). When imaging, an evenly illuminated scene is used as the flat field. We take $N_f = 10$ quarz lamp spectra of 60 sec exposures at the beginning of each night and we co-add them using the *flatcombine* task to obtain a calibration flat field frame: <

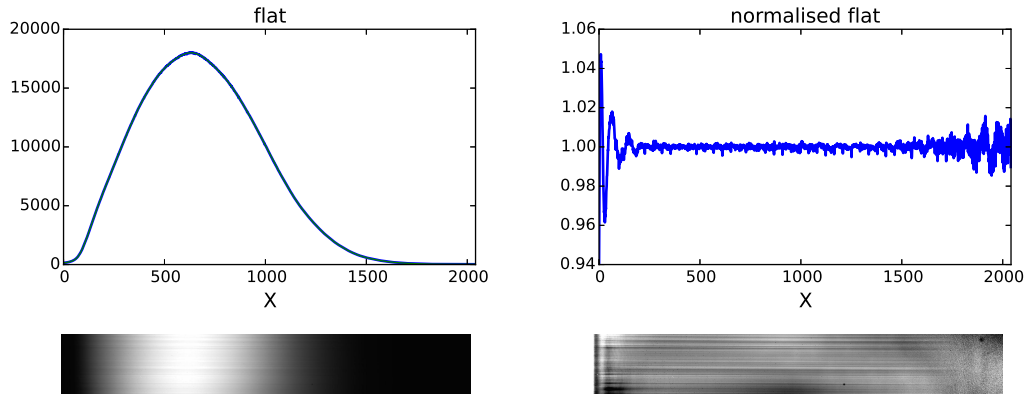

Figure 1.2: Top panels: A section through a typical flat field for spectroscopy (left) and the same flat field after the large-scale curve has been divided out (right). Bottom left panel: median spectroscopic flat field (10 images used); Bottom right panel: as on the right but after normalising the image by removing the overall lamp spectrum shape. The typical fringing pattern is visible in the lower part of both panels;it is caused by interference of multiple reflections between the two surfaces of the CCD. Even if the fringing pattern is visible in the spectroscopic flat, it is not fully removed by it, since it is an additive component and not a multiplicative one.

$FLAT >= \frac{1}{N_f}\sum_i^{N_f}(Flat_i - OS_i) - < BIAS >$. An example is shown in the bottom left panel of Figure 1.2. To remove the response of the lamp, a low-order curve is fitted using the *response* task to the spectrum of the flat frame -if the spectrum runs with dispersion parallel to the X-axis, we collapse the flat-field frame by summing any number of columns, producing a 1D spectrum for the lamp. The top left panel in Figure 1.2 shows how one of these spectra appears. The spectrum has a simple, continuous shape with small-scale noise superimposed. Having fitted a curve, we divide the flat-field by it so as to leave the small-scale sensitivity variations only (see right panels of Fig.1.2 for the 1D and 2D normalised flats). We divide each data frame by the normalised (to 1 DN) calibration flat frame where the difference between the value in the pixel and unity gives the percent variation from the mean gain using the *ccdproc* task.

We have finally obtained the clean data frames:

$$[DATA] = \frac{[RAW] - OS - < BIAS >}{< FLAT >} \quad . \tag{1.1}$$

We ignore the thermal dark current that is caused by thermally generated electrons (order of a few electrons/hour) because our integration times are $\sim$ 10 minutes.

1.2.3 Cosmic rays removal

We remove cosmic rays (CRs) from individual frames using the L.A. Cosmic algorithm (van Dokkum, 2001) built for robust cosmic ray identification. It detects cosmic rays of arbitrary shapes and sizes,

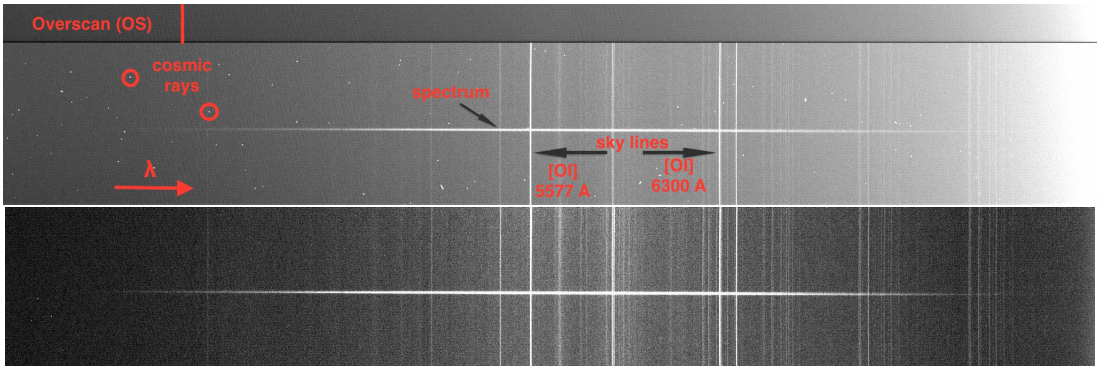

Figure 1.3: Top image: Example of a 2D science frame before applying the data reduction steps. The overscan region is used for measuring the amplifier bias level. The object spectrum is situated horizontally in the middle of the frame and the sky lines are perpendicular to it. The small white spots are cosmic rays that are eliminated in the data reduction. Bottom image: Same science frame as above but after applying the data reduction steps. From this image we extract the 1D spectrum we use to measure the HAC radial velocities.

and distinguishes between undersampled point sources and cosmic rays. We use the task `lacos_im` for which we need to specify the sigma level above which the CRs are removed: it sigma is too low, all the CRs are removed but also some fainter sky lines; if it is high, you may not remove all the CRs. We estimate that a good detection limit for cosmic rays is $\sigma = 14$.

1.2.4 Aligning multiple images

The targets on the first night were observed using only one exposure. For other nights we build up signal to noise by using two or three exposures. Unlike flats, there is an extra step in combining several science exposures: alignment. The images can be slightly offset from one another due to the shift of the star along the slit, so we need to align them. To do this, we sum all columns along the wavelength axis and we fit a Gaussian to determine the position of the star on the slit. We shift all subsequent exposures to match the position of the first one using the *imshift* task.

1.2.5 Spectrum extraction

From the clean data frames (e.g. bottom panel of Fig. 1.3) we extract the 1D spectra that needs to be converted to a wavelength scale (see next subsection). For this we use the *apall* task that extracts the spectrum from the 2D CCD image.

If we plot the pixel values along the columns of the image, the spectrum will appear as a peak. Using *apall* we define an aperture centred on the dispersion axis with a width that gathers all of the light in the spectrum. After defining the aperture, we set the background apertures where we fit the background. Apall determines also the shape of the aperture (or trace) along the dispersion axis and it fits it with a

polynomial.

There are two ways of extracting the spectrum: we could simply add up all of the counts in the aperture and subtract off the background or we could do a variance weighting in which the sum is weighted by the signal to noise in that pixel. The first procedure is known as a simple or linear extraction. In many cases such an extraction is not adequate and does not make the most of the data available as it does not take into account that the small numbers of photons in the wings increases the noise. The second method (or 'optimal extraction') is more resistant to a few noisy pixels and does a pretty good job rejecting cosmic rays. In this work, we employed the second method. The readout noise and the gain of the CCD are needed to calculate pixel weights. The gain is used to convert the data in the input images, which are in units of counts, to the number of recorded photons. Once we have the data in these units, we can apply an error-based weighting to the summation of data in each sample along the dispersion direction. A profile curve can then be fitted to the spectrum in the spatial direction. At the centre of the profile the signal is greatest; on the outside, the signal falls off to the background level. If we had summed these pixels in an unweighted manner we would be ignoring the fact that the central pixels have a better signal-to-noise ratio as compared to those at the outside. For suitable data, optimal extraction also acts as a cosmic-ray filter: any pixel which deviates strongly from the profile model is likely to be contaminated by a cosmic ray and can be rejected.

The same extraction is applied to both the target and the arc frames.

1.2.6 Wavelength calibration

After extracting every spectrum, we need to generate a wavelength solution, which means that we will determine the mapping between pixel number along the spectrum and wavelength, using the arc lamps that we have obtained throughout each night. We use the *identify* task to associate the lines Ar, Ne, Xe, Hg with features in the calibration lamp exposure and the *dispcor* task to associate that wavelength solution with the science exposures to which it applies. The arc exposures are extracted using the same profile weights as for the object to ensure any tilt/rotation is the same. The line positions in pixels are fitted with a third order spline, to retrieve the dispersion relation λ=f(pix). In is important that the arcs are obtained before observing each RR Lyrae since flexures in the telescope/spectrograph system causes wavelength drifts as a function of time and position of the telescope. Typically, the resulting wavelength solution should be good to a fraction of a pixel as we can measure the centroid of spectral lines to very high precision given sufficient S/N, well below the 2 $\mathring{A}$ per pixel spectral resolution.

Our purpose is to find radial velocities, so we are interested only in calculating a shift in wavelength, so

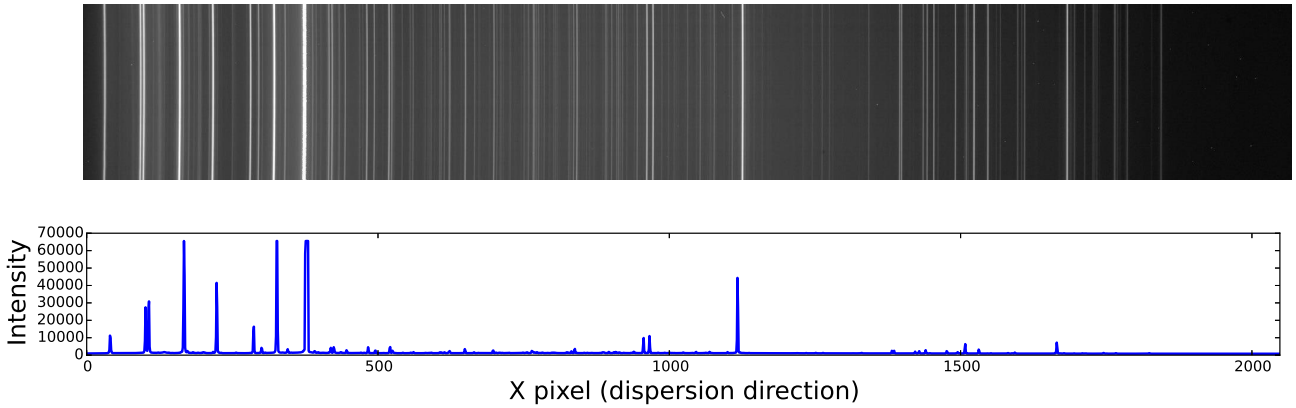

Figure 1.4: An example of an arc lamp, with Ar, Xe, Ne and Hg lamps turned on. Arc lamp exposures 120 seconds long were taken before observing each target since flexures in the telescope/spectrograph system causes drifts as a function of time and position of the telescope.

we do not transform from counts to intensity.

1.2.7 Radial velocity correction for Earth's motion

When making spectrographic observations with the intention of calculating radial velocities we need to consider that we are sitting on a moving platform. The motion of the Earth with respect to the barycentre of the Solar system (or the heliocentre which is essentially equivalent) must be calculated and accounted for. This correction must account for the rotation and orbital motion of the Earth. This can be done using the *rvcorrect* task. For this task we need to specify the observatory where the observations were taken (as this will effect the heliocentric velocity correction) and the year, month, day, and Universal Time of each observation, together with the right ascension and declination of the target. To remove the Earth's motion toward/away from the star, we need to subtract this velocity, and this is done with the *dopcor* task.

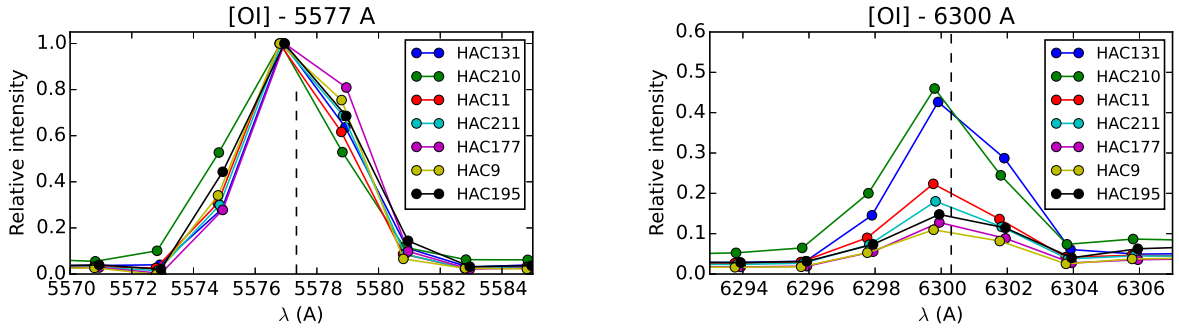

Figure 1.5: O I sky emission lines help with the radial velocity by showing possible systematic offsets. We show the sky lines for 7 targets observed during the second night of observations. The centers of the lines match well the catalogue values of the [OI] sky lines in the air, $\lambda_0 = 5577,6300$ Å.

Table 1.1: $< \sigma_{log_{10}(\lambda_{obs})} >$ is the mean of the line widths in log space $\sigma_{log_{10}(\lambda_{obs})}$ obtained for the targets during the night; σ_{cal} are the calibration errors for each night of observations.

night	$< \sigma_{log_{10}(\lambda_{obs})} >$	σ_{cal} (km/s)
n1	-9.46e-05	12.7
n2	-9.26e-05	8.4
n3	-8.85e-05	9.8
n4	-3.62e-06	14.2
n5	-3.80e-06	9.1
n6	-9.91e-05	3.9

1.2.8 Calibration errors

We use the [OI] sky emission lines to identify any systematic offsets in the radial velocity determination. We fit the 5577 and 6300 $\mathring{\text{A}}$ [OI] lines (see Fig. 1.5) in $log_{10}(\lambda)$ space with Gaussians, for each star, to calculate the centre of each line, $log_{10}(\lambda_{obs})$ and the standard deviation $\sigma_{log_{10}(\lambda_{obs})}$. We calculate the error in velocity a wrong calibration would produce, using the Doppler formula : $\lambda_{obs} = \lambda_0(1+v/c)$ which in log space is the linear equation: $log_{10}(\lambda_{obs}) = log_{10}(\lambda_0) + log_{10}(1+v/c)$ with $\lambda_0 = 5577,6300$ $\mathring{\text{A}}$ for the [OI] sky lines in the air. Assuming the calibration errors are random, the standard deviation of the v_{obs} distribution will give us the calibration error σ_{cal} and the centre of the distribution the systematic offset between v_0 in the Earth's reference frame and the calibration.

The resolution of our instrument is $R = \lambda/FWHM \sim 1700$. In the next section we will use synthetic spectra with $R = 20,000$ which we degrade with a Gaussian convolution with constant $\sigma =< \sigma_{log10(\lambda_{obs})} >$ in $log(\lambda)$ space, calculated to be the mean of the $\sigma_{log10(\lambda_{obs})}$ obtained for the targets during the night. These values are reported in the second column of Table 1.1 for each night.

1.3 Velocity determination and spectral fitting

In this section we measure the centre of mass velocity of the RR Lyrae (or systemic velocity v_{sys}), that is the line of sight velocity the star would have had if its atmosphere were at rest. First, we need to measure the heliocentric radial velocities (v) from the extracted 1D spectra and then use the phase of each observation to find the true systemic velocity .

To find the heliocentric radial velocity, we use direct pixel-fitting methods which have been widely employed for more than a decade in spectroscopic studies of unresolved stellar populations as well as observations of individual stars (e.g. Cappellari and Emsellem 2004; Koleva et al. 2009). Methods based on direct pixel fitting provide more realistic error bars and give a better way to treat multiple templates and continuum levels. Moreover, with this method, the original observed spectrum is neither

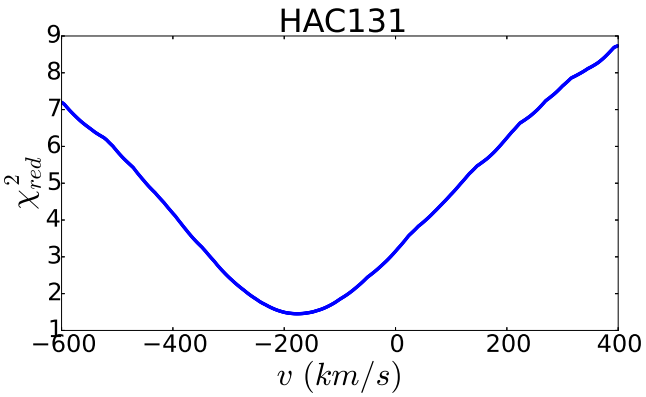

Figure 1.6: Reduced chi-square of the spectral fit as a function of radial velocity, using the best template for the H_α and H_β lines.

rebinned nor interpolated in any way, thus preserving all the information. An important ingredient for direct pixel-fitting methods is the library of template spectra. We use 90 synthetic spectra selected from Munari et al. (2005). The templates in the library have a step size of 1 Å per pixel and cover a large range of stellar parameters: $-2.5 < [Fe/H] < 0.5; [\alpha/Fe] = 0, 0.4; 3,000 < T_{eff}/K < 80,000; 1.5 < log(g) < 5; 0 < V_{rot}/(km/s) < 150$. While synthetic spectral libraries have obvious limitations and we do not expect a perfect match to the observed stars, the range of stellar parameters covered in the library is large and is significantly better than what we can achieve with stellar libraries of high-resolution spectra for real stars. We choose a subsample of templates with atmospheric parameters that match the typical properties of RR Lyrae stars as in Table 1.2. In a first iteration we used 208 templates for a wide range of parameters but the results were almost identical to the ones reported here (variations up to ~ 4 km/s, smaller than the calibration errors) so for computational speed we choose to work with the smaller sample of 90 templates.

We resample the templates to the dispersion of the observed spectrum (2 Å per pixel) and convolve them with a Gaussian Line Spread Function with constant $< \sigma_{log10(\lambda_{obs})} >$ listed in Table 1.1 for each night. We fit simultaneously two spectral regions of the spectrum, one centred on H_β (4811 - 4911 Å) and one on H_α (6512 - 6612 Å) shown in blue in Fig 1.7. Having the stellar template library we construct the model of each observed spectrum as

$$Model = P(\lambda) T_i(\lambda(1 + v/c)), \tag{1.2}$$

where $T_i(\lambda)$ is the ith resampled template spectrum from the template grid convolved with the appropriate line spread function LSF(λ) with $\sigma_{log10(\lambda_{obs})}$, v is the radial velocity of the object, and $P(\lambda) = \sum_{j=0}^{N-1} p_j \lambda^j$ is the normalising polynomial of degree N, which takes into account the lack of flux cali-

Table 1.2: List of typical RR Lyrae properties, taken from RR Lyrae Stars by Horace A. Smith. The rows are, in order, typical mass and typical radius, period of pulsation, time averaged absolute magnitude, time averaged surface temperature, the log of the time averaged surface gravity, the iron to hydrogen abundance ratio. We chose the parameters for the library of template spectra (Munari et al. 2005) employed in the pixel-fitting method to closely match the typical values for RR Lyrae.

	Properties of RR Lyrae	Selected templates
Mass	0.7 $M_\odot$	
Radius	4-6 $R_\odot$	
Period	0.2 - 1.1 days	
M_V	0.6 ± 0.2	
T_{eff}	6100 K - 7400 K	5500 K - 7500 K
log (g)	[2.5, 3.0]	2.5, 3.5
$[Fe/H]$	[0 , -2.5]	[-0.5, -2.5]

bration of our spectra as well as uncertainty in the spectral continuum. In fact, we are not interested in values of the coefficients of the normalising polynomials, so in the following discussion we do not mention them further. We found that $N = 15$ worked well for all targets. Having the spectral model we can then compute the χ^2 values by summing scaled residuals over pixels:

$$\chi^2 = \sum_k \left(\frac{S_k - Model(\lambda_k)}{Sig_k}\right)^2 \tag{1.3}$$

where S_k and Sig_k are the observed spectra and sigma spectra respectively, and the k are the wavelengths of the pixels of the extracted spectra. The sigma spectra are produced with IRAF during the spectrum extraction procedure. Model(λ_k) is the evaluation of the synthetic stellar model spectrum at the wavelengths of the individual pixels. For each template $T_i(\lambda(1+v/c))$ we calculate the χ_i^2 on a grid of velocities v between -600 and +400 km/s with a step of 1 km/s. The best fit template T_i is then the one that produces the minimum χ_i^2 at the best fit velocity v of the template. In Fig. 1.6 we show the reduced chi square χ^2_{red} as a function of velocity. In Table 1.3 we report the best fit velocities v for all the observed targets for one particular object. The uncertainty in the best fit v is determined from the chi-square distribution (e.g. Fig. 1.6) near the minimum, more specifically from the second derivative of the chi square function: $\sigma_v = 1/\sqrt{d^2\chi^2/dv^2}$.

Although the fitting is motivated by optimising the radial velocity accuracy, and not primarily by measuring the stellar astrophysical parameters T_{eff}, $log(g)$, and $[Fe/H]$, the values of the parameters determined from the best-fit templates are reasonable. Figure 1.9 shows how the best fit template parameters correlate with radial velocities v. The temperature range of RR Lyrae is given for both RRab and RRc stars in Table 1.2, but the latter have higher effective temperatures than the first so finding $T_{eff} \approx 6250$K is not surprising for our sample of RRab.

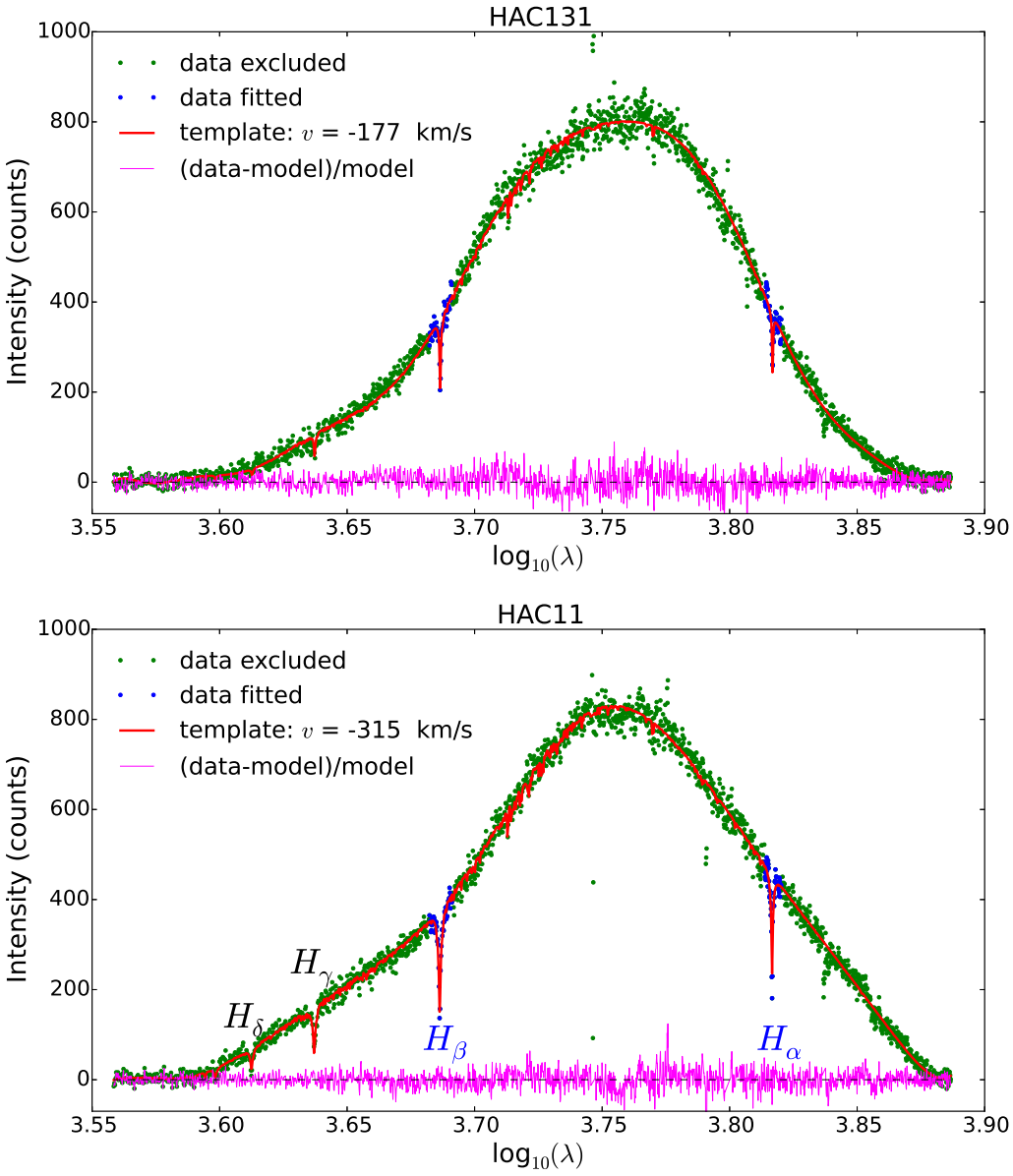

Figure 1.7: Spectra of targets HAC131 and HAC11 and best fit templates. Four of the Balmer lines are in the technically "visible" part of the spectrum, with wavelengths longer than 400 nm and shorter than 700 nm but the fit was done only on the H_α and H_β lines (shown in blue). The templates shown have the best velocity, temperature, log(g) and metallicity obtained from the fit of the H_α and H_β lines but the polynomial was refitted on the full spectrum just for illustration purposes.

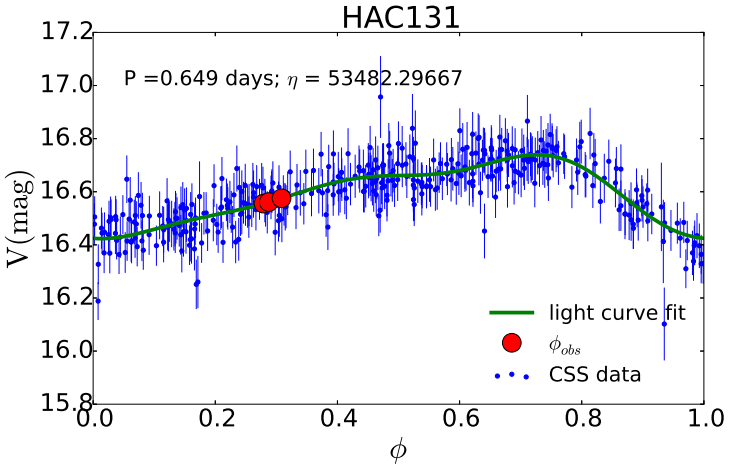

Figure 1.8: Light curve of RRab HAC131. The light curve is shifted so that at phase 0 the RRL has maximum brightness. In red we show the tree different phases (3 exposures of 600 s) at which the star was observed.

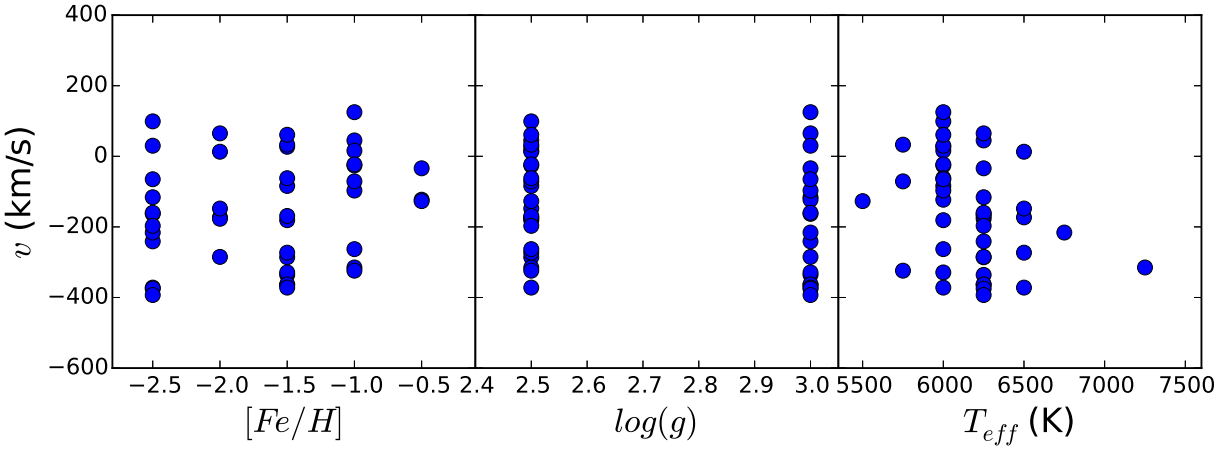

Figure 1.9: Stellar parameters determined from our synthetic spectrum template fit. The left panel shows the 2D histogram of radial velocities and metallicities of the best-fit templates for all observed stars.

For each star, we apply our fitting procedure to the co-added spectra from each exposure. RR Lyrae stars are dimmer near phase 0.5 (0.3-0.5 mag compared to maximum light at phase of zero -ephemeris-), and thus require longer exposures to reach the same signal-to-noise ratio.An example of a CSS light curve is shown in Figure 1.8 where the observed phases are marked in red. The danger of longer exposures is blurring of spectral lines due to pulsations, which in turn decreases the precision of radial velocity measurements.

To find the systemic velocity we now need to subtract the velocity due to pulsations. If we observed the RR Lyrae stars at a particular point during a pulsation period when the observed radial velocity is presumed to be equal to the stars systemic velocity (usually phase 0.5), then we wouldn't need to apply any corrections. However it is difficult to time the observations in such a way to make them when $\phi_{obs} = 0.5$ so stars are observed at different phases: we need to use templates build by Sesar (2012) that describe the changes in radial velocity due to pulsations as a function of pulsation phase, to determine the velocity correction. We calculate the phase of the star at the time of the observation with $\phi_{obs} = mod((MJD_{obs} - \eta), P)/P$ where η is the ephemeris (the MJD of maximum brightness) and P is the period of the light curve given by Drake et al. (2013a) and MJD_{obs} is the Modified Julian Date. Knowing the phase at which we observed the RRL, ϕ_{obs}, we interpolate the templates T (figure 1 in Sesar et al. 2012) that measure normalised and phased radial velocity curves obtained from measurements H_α line (top right panel), H_{beta} line (bottom left panel) and find $T(\phi_{obs})$. In each panel, the solid line shows a B-spline curve interpolated through normalised radial velocities (i.e., the template radial velocity curve). The template and the normalised radial velocities are offset so the velocity at phase 0.5 (the phase at which the radial velocity is presumed to be equal to the systemic velocity) is equal to zero. These templates do not cover the full range of phases, but end at phase of 0.95 as the radial velocities change very rapidly between phases of 0.95 and 1.0. This should not be a problem as the velocities measured from Balmer lines between these phases are in general more uncertain, mainly due to increased spectral blurring (i.e., due to a rapid change in velocity as a function of time), and are not very useful.

There is a tight correlation between the amplitudes of Balmer lines velocity curves, A_{rv}, and V-band light curves amplitudes A_V. Sesar (2012) reports the following relation between the velocity amplitudes and the V-band light-curve amplitudes:

$$A^{\alpha}_{rv} = 35.6A_V + 78.2$$

$$A^{\beta}_{rv} = 42.1A_V + 51.1$$

This suggests that, in theory, the most precise systemic velocity may be obtained by averaging systemic velocities, that are measured from individual Balmer lines. However, because our stars are faint, we simultaneously fit the H_α and H_β lines with the template spectrum. Due to the fact that Balmer line velocity curves have different shapes and amplitudes, we expect that such measurements may be more uncertain. Sesar 2012 estimate the level of uncertainty introduced by using more than one Balmer line in a cross-correlation, and in their figure 3 show the standard deviation of radial velocities of various Balmer lines as a function of phase for RR Lyrae stars with different V-band amplitudes. In general, the uncertainty in velocity introduced by using more than one Balmer line in a cross-correlation is lowest for phases earlier than 0.6 , and it decreases with increasing V-band amplitude.

Finally, the observed radial velocity v_{sys} can be calculated as:

$$v_{sys} = v - v_{puls} \tag{1.4}$$

with the velocity due to pulsations

$$v_{puls} = \frac{A^{\alpha}_{rv} T_\alpha(\phi_{obs}) + A^{\beta}_{rv} T_\beta(\phi_{obs})}{2} \tag{1.5}$$

where A_{rv} is the amplitude of the radial velocity curve and $T(\phi_{obs})$is the template radial velocity curve, ϕ_{obs} is the phase of the observation , v is the observed velocity and v_{sys} is the systemic velocity. We calculate v_{puls} for each phase when we have multi exposures and average the values we obtain and subtract that value from the velocity v found from the fitting of the co-added spectra.

From figure 3 in Sesar et. al 2012 (solid blue line when H_α and H_β are used) that shows the uncertainty in velocity introduced more than one Balmer line in the velocity determination, we estimate the error introduced by subtracting the velocity due pulsations: $\sigma_{puls} = 2$ km/s for $\phi_{obs} < 0.4$, $\sigma_{puls} = 0$ km/s for $\phi_{obs} \approx 0.5$ and increases linearly up to 14 km/s.

The final error reported in Table 1.3 is $\sigma_{tot} = \sqrt{\sigma^2_{fit} + \sigma^2_{puls} + \sigma^2_{cal}}$. In the table we also list the velocity corrections calculated individually from the H_α and H_β lines and we notice they are not very different, therefore fitting simultaneously two lines does not introduce an significant error on the final result.

Drake et al. 2013 matched the locations of all the RRL in CSS with the SDSS within a 3" radius and obtained a sample of 7,788 sources with SDSS photometry (table 2 in Drake et al. 2013); 905 of them have spectra with a resolution of $R \sim 2000$ and S/N$\sim$25. One of these is within our selection criteria for HAC candidates (1 in 225 candidates) and is shown in magenta in Figure 1 and is reported on the last line of Table 1.3 even though we do not know the ϕ_{obs} so some information is missing. Drake et al. 2013 also used the relationships given by Sesar (2012) to produce velocity corrections for the

SDSS measurements. He determined pulsation corrections for each of the 905 spectra by averaging the velocities over the period between the start and the end phase of the SDSS observations. They have compared the distribution of differences in RRab radial velocities calculated from pairs of SDSS spectra before and after pulsation corrections pulsation: before the corrections the differences had a Gaussian distribution of $\sigma = 20$ km/s and after, a much smaller σ= 14.3 km/s. This is the error reported on the v_{GSR} for the SDSS target in the table. We have observed three targets twice at different phases (see Table 1.4) HAC195, HAC197 and HAC211. HAC211 ('n2') and HAC197('n4') have 'extreme' phases ϕ_{obs} (smaller that 0.1 or bigger than 0.95) where the velocity corrections are unreliable so we cannot compare the final velocities but the v_{sys} values we obtain for *HAC*195 are consistent.

night	name	ϕ_{obs}	v	χ^2_{red}	$A^{H_\alpha}_{rv}T_{H_\alpha}$	$A^{H_\beta}_{rv}T_{H_\beta}$	v_{sys}	v_{gsr}	σ_{tot}	type
			km/s		km/s	km/s	km/s	km/s	km/s	
n1	HAC211	0.608	-286	1.06	15.6	10.3	-299.0	-168.6	21.75	OoII
n1	HAC197	0.1048	-174	1.3	-48.0	-44.4	-127.8	2.6	14.85	OoI
n1	HAC59	0.0995	-362	1.41	-52.8	-50.9	-310.1	-198.0	14.76	OoI
n1	HAC37	0.5106	-336	1.53	2.0	1.8	-337.9	-220.7	13.86	OoI
n1	HAC152	0.5095	-183	1.49	1.5	1.3	-184.4	-30.1	15.56	OoI
n1	HAC22	0.5052	98	1.25	0.9	0.8	97.2	230.1	15.63	OoII
n1	HAC27	0.1084	-32	1.47	-48.5	-45.3	14.9	115.3	15.83	OoI
n1	HAC186	0.4982	-23	1.24	-0.3	-0.3	-22.7	99.6	16.61	OoI
n1	HAC91	0.5047	-241	1.69	0.7	0.6	-241.7	-131.3	15.88	OoII
n1	HAC195	0.0901	-383	1.16	-47.4	-42.7	-338.0	-226.1	14.99	OoI
n2	HAC26	0.3661	-364	1.25	-20.4	-20.3	-343.6	-222.0	15.29	OoI
n2	HAC131	0.3085	-177	1.45	-22.9	-20.7	-153.5	-3.2	14.88	OoI
n2	*HAC210*	0.0304	119	1.26	-66.3	-66.7	186.1	292.1	16.58	OoI
n2	HAC11	0.1164	-315	2.06	-52.8	-52.1	-261.9	-141.3	12.26	OoI
n2	*HAC211*	0.947	-320	2.0	38.1	19.5	-348.8	-218.4	17.64	OoII
n2	HAC177	0.1032	45	1.81	-48.2	-44.5	91.8	234.3	12.51	OoI
n2	HAC9	0.5026	27	1.88	0.4	0.3	27.4	161.9	12.26	OoI
n2	HAC195	0.5046	-329	2.97	0.6	0.5	-329.0	-217.2	12.63	OoI
n2	HAC96	0.1155	-148	2.11	-50.4	-48.6	-97.9	51.8	10.94	OoI
n2	HAC105	0.1139	-273	2.05	-46.1	-42.1	-228.5	-90.7	11.23	OoI
n2	HAC102	0.4887	125	2.2	-1.8	-1.5	127.2	235.8	13.88	OoII
n2	HAC145	0.5108	16	1.84	1.8	1.5	16.0	140.9	11.5	OoI

n3	HAC51	0.6	-324	1.82	17.7	13.1	-337.6	-168.4	15.35	OoI
n3	HAC45	0.7213	-163	1.77	34.3	20.7	-190.1	-31.6	20.83	OoI
n3	HAC52	0.532	-363	1.71	5.7	4.7	-366.1	-217.6	15.56	OoI
n3	HAC42	0.1131	13	1.47	-47.7	-44.4	59.4	199.9	13.55	OoI
n3	HAC156	0.5376	33	1.92	6.5	5.3	29.5	149.7	14.56	OoI
n4	*HAC204*	0.9028	64	1.47	39.3	20.3	34.3	141.4	23.48	OoI
n4	HAC94	0.6281	-263	1.69	22.5	16.1	-280.7	-131.3	16.5	OoI
n4	HAC191	0.5205	-116	1.56	3.7	3.2	-117.3	14.9	19.27	OoI
n4	HAC194	0.5425	-372	1.54	6.9	5.4	-375.4	-239.7	18.33	OoI
n4	HAC218	0.0778	82	1.23	-49.2	-44.5	129.3	227.7	16.12	OoI
n4	HAC21	0.5129	-84	1.48	1.8	1.4	-85.0	47.3	15.23	OoI
n4	HAC208	0.6435	65	1.46	24.8	17.2	44.6	167.4	17.43	OoI
n4	HAC166	0.5222	-23	1.57	3.1	2.4	-24.4	86.9	17.26	OoI
n4	HAC154	0.5205	-372	1.77	3.0	2.4	-374.1	-276.4	15.86	OoI
n4	HAC120	0.5166	30	1.76	2.3	1.8	28.7	127.9	16.52	OoI
n4	HAC121	0.1209	-216	1.9	-48.3	-45.8	-168.3	-22.8	15.71	OoI
n4	*HAC197*	0.0002	-163	1.58	-58.3	-53.9	-150.3	-19.8	15.27	OoI
n4	HAC187	0.8679	82	1.51	41.1	21.8	50.7	190.5	19.03	OoI
n4	HAC189	0.0652	-481	1.68	-51.0	-46.4	-431.8	-294.6	15.33	OoI
n4	HAC169	0.4298	-123	1.46	-11.7	-11.3	-109.3	33.9	17.54	OoI
n5	HAC31	0.5134	-375	1.31	2.5	2.2	-375.0	-223.5	13.71	OoI
n5	HAC48	0.4959	61	1.38	-0.7	-0.6	63.2	234.8	13.66	OoI
n5	HAC115	0.5272	-169	1.75	4.5	3.6	-171.2	-9.8	13.83	OoI
n5	HAC60	0.8426	-160	1.35	47.0	26.8	-196.7	-58.8	16.46	OoI
n5	HAC158	0.6726	-285	1.59	24.8	15.1	-304.6	-172.7	13.3	OoI
n5	HAC113	0.673	-127	3.13	29.7	19.7	-151.2	-26.2	18.85	OoII
n5	HAC71	0.4947	-393	1.57	-0.9	-0.8	-390.3	-247.0	12.05	OoI
n5	*HAC76*	0.9257	77	2.11	43.6	23.9	43.4	155.4	16.6	OoI
n5	HAC87	0.0678	-102	1.28	-55.2	-52.7	-46.8	69.8	14.69	OoI
n5	HAC47	0.6665	-97	2.1	27.3	17.9	-118.3	7.6	12.25	OoI
n5	HAC163	0.0782	-193	2.2	-59.6	-59.4	-132.8	-14.6	10.62	OoI
n5	HAC126	0.5857	-197	1.57	14.3	10.5	-208.1	-72.2	14.9	OoI
n5	*HAC80*	0.0093	-265	1.88	-70.2	-71.3	-249.0	-95.8	11.24	OoI

n5	HAC169	0.5426	-71	1.28	7.7	6.3	-77.3	65.9	19.46	OoI
n5	HAC82	0.4777	-62	1.47	-3.4	-3.0	-57.6	103.0	14.44	OoII
n6	HAC143	0.5346	-65	1.75	4.9	3.6	-68.1	81.9	14.55	OoI
SDSS	HAC184	-	-	-	-	-	-	5.3	14.3	OoI

Table 1.3: The 225 potential HAC targets were selected using the following selection criterium: 28< l < 55 , -45< b <-20 , V <17.5, 15< D < 20 kpc. 55 of these targets were observed, 3 of which twice (listed in Table 2). 13 of the observed targets ['HAC59', 'HAC195', 'HAC210', 'HAC211', 'HAC204', 'HAC218', 'HAC197', 'HAC187', 'HAC189', 'HAC76', 'HAC87', 'HAC163', 'HAC80' , ['n1', 'n1', 'n2', 'n2', 'n4', 'n4', 'n4', 'n4', 'n4', 'n5', 'n5', 'n5', 'n5'] were eliminated after a second selection criterium was applied: $0.1 < \phi_{obs} < 0.85$, used to discard the stars where the pulsation velocity corrections are uncertain. Some of these were duplicates so a total of 45 targets remains. One of the 225 HAC candidates was observed by SDSS and we include it in our sample. Because some information about this target is missing, it will be excluded from some plots. 87% of the targets in the 'clean' sample belong to the Oo I population, while 81% of all the CSS stars in the same sky area are Oo I type.

night	name	ϕ_{obs}	$v_{template}$	χ^2_{red}	$A^{\alpha}_{rv}T_{\alpha}$	$A^{\beta}_{rv}T_{\beta}$	v_{sys}	v_{gsr}	σ_{tot}	
n1	HAC211	0.608	-286.0	1.06	15.6	10.3	-299.0	-161.1	21.75	OoII
n2	*HAC211*	0.947	-319.0	30.95	38.1	19.5	-347.8	-209.9	16.42	OoII
n1	HAC197	0.1048	-174.0	1.3	-48.0	-44.4	-127.8	12.1	14.85	OoI
n4	*HAC197*	0.0002	-163.0	33.3	-58.3	-53.9	-150.3	-10.3	14.84	OoI
n1	HAC195	0.0901	-383	1.16	-47.4	-42.7	-338.0	-226.1	14.99	OoI
n2	HAC195	0.5046	-329	2.97	0.6	0.5	-329.0	-217.2	12.63	OoI

Table 1.4: Properties of the duplicate targets. The only target observed at borderline 'acceptable' phases is HAC195: the velocities after pulsation correction v_{sys} from the two nights after radial velocity pulsation corrections, agree within one sigma.

Bibliography

Aguerri, J. A. L., Méndez-Abreu, J., and Corsini, E. M.: 2009, *AA* **495**, 491

Alard, C.: 2001, *AA* **379**, L44

Aparicio, A. and Gallart, C.: 2004, *AJ* **128**, 1465

Athanassoula, E.: 2003, *MN* **341**, 1179

Athanassoula, E.: 2005, *MN* **358**, 1477

Babusiaux, C. and Gilmore, G.: 2005, *MN* **358**, 1309

Bahcall, J. N. and Soneira, R. M.: 1980, *ApJS* **44**, 73

Bekki, K. and Freeman, K. C.: 2003, *MN* **346**, L11

Belokurov, V.: 2013a, *arXiv:1307.0041* **57**, 100

Belokurov, V.: 2013b, *New Astronomy Reviews* **57**, 100

Belokurov, V., Evans, N. W., Bell, E. F., Irwin, M. J., Hewett, P. C., Koposov, S., Rockosi, C. M., Gilmore, G., Zucker, D. B., Fellhauer, M., Wilkinson, M. I., Bramich, D. M., Vidrih, S., Rix, H.-W., Beers, T. C., Schneider, D. P., Barentine, J. C., Brewington, H., Brinkmann, J., Harvanek, M., Krzesinski, J., Long, D., Pan, K., Snedden, S. A., Malanushenko, O., and Malanushenko, V.: 2007a, *ApJL* **657**, L89

Belokurov, V., Evans, N. W., Irwin, M. J., Lynden-Bell, D., Yanny, B., Vidrih, S., Gilmore, G., Seabroke, G., Zucker, D. B., Wilkinson, M. I., Hewett, P. C., Bramich, D. M., Fellhauer, M., Newberg, H. J., Wyse, R. F. G., Beers, T. C., Bell, E. F., Barentine, J. C., Brinkmann, J., Cole, N., Pan, K., and York, D. G.: 2007b, *ApJ* **658**, 337

Belokurov, V., Zucker, D. B., Evans, N. W., Gilmore, G., Vidrih, S., Bramich, D. M., Newberg, H. J., Wyse, R. F. G., Irwin, M. J., Fellhauer, M., Hewett, P. C., Walton, N. A., Wilkinson, M. I., Cole, N., Yanny, B., Rockosi, C. M., Beers, T. C., Bell, E. F., Brinkmann, J., Ivezić, Ž., and Lupton, R.: 2006, *ApJL* **642**, L137

Binney, J., Gerhard, O., and Spergel, D.: 1997, *MN* **288**, 365

Bissantz, N. and Gerhard, O.: 2002, *MN* **330**, 591

Blažko, S.: 1907, *Astronomische Nachrichten* **175**, 327

Blitz, L. and Spergel, D. N.: 1991, *ApJ* **379**, 631

Bovy, J., Rix, H.-W., and Hogg, D. W.: 2012, *ApJ* **751**, 131

Bressan, A., Marigo, P., Girardi, L., Salasnich, B., Dal Cero, C., Rubele, S., and Nanni, A.: 2012, *MN* **427**, 127

Broyden, A.: 1970, *Journal of the Institute of Mathematics and Its Applications* **6**, 76

Bruzual, G., Barbuy, B., Ortolani, S., Bica, E., Cuisinier, F., Lejeune, T., and Schiavon, R. P.: 1997, *AJ* **114**, 1531

Bullock, J. S. and Johnston, K. V.: 2005, *ApJ* **635**, 931

Bureau, M., Aronica, G., Athanassoula, E., Dettmar, R.-J., Bosma, A., and Freeman, K. C.: 2006, *MN* **370**, 753

Byrd, R. H.and Lu, P., Nocedal, J., and Zhu, C.: 1995, *SIAM J. Sci. Comput.* **16**, 1190

Cappellari, M. and Emsellem, E.: 2004, *PASP* **116**, 138

Cardelli, J. A., Clayton, G. C., and Mathis, J. S.: 1989, *ApJ* **345**, 245

Catelan, M.: 2009, *ApSS* **320**, 261

Catelan, M. and Cortés, C.: 2008, *ApJL* **676**, L135

Chaboyer, B.: 1999, *Post-Hipparcos Cosmic Candles* **237**, 111

Chabrier, G.: 2001, *ApJ* **554**, 1274

Chabrier, G.: 2003, *PASP* **115**, 763

Chen, B. Q., Schultheis, M., Jiang, B. W., Gonzalez, O. A., Robin, A. C., Rejkuba, M., and Minniti, D.: 2013, *AA* **550**, A42

Clement, C. M., Muzzin, A., Dufton, Q., Ponnampalam, T., Wang, J., Burford, J., Richardson, A., Rosebery, T., Rowe, J., and Hogg, H. S.: 2001, *AJ* **122**, 2587

Dalcanton, J. J. and Bernstein, R. A.: 2002, *AJ* **124**, 1328

Deason, A. J., Belokurov, V., and Evans, N. W.: 2011, *MN* **416**, 2903

Debattista, V. P. and Sellwood, J. A.: 2000, *ApJ* **543**, 704

Dehnen, W. and Binney, J. J.: 1998, *MN* **298**, 387

Di Matteo, P., Haywood, M., Gómez, A., van Damme, L., Combes, F., Hallé, A., Semelin, B., Lehnert, M. D., and Katz, D.: 2014a, *AA* **567**, A122

Di Matteo, P., Haywood, M., Gómez, A., van Damme, L., Combes, F., Hallé, A., Semelin, B., Lehnert, M. D., and Katz, D.: 2014b, *AA* **567**, A122

Dotter, A., Sarajedini, A., Anderson, J., Aparicio, A., Bedin, L. R., Chaboyer, B., Majewski, S., Marín-Franch, A., Milone, A., Paust, N., Piotto, G., Reid, I. N., Rosenberg, A., and Siegel, M.: 2010, *ApJ* **708**, 698

Drake, A. J., Catelan, M., Djorgovski, S. G., Torrealba, G., Graham, M. J., Belokurov, V., Koposov, S. E., Mahabal, A., Prieto, J. L., Donalek, C., Williams, R., Larson, S., Christensen, E., and Beshore, E.: 2013a, *ApJ* **763**, 32

Drake, A. J., Catelan, M., Djorgovski, S. G., Torrealba, G., Graham, M. J., Mahabal, A., Prieto, J. L., Donalek, C., Williams, R., Larson, S., Christensen, E., and Beshore, E.: 2013b, *ApJ* **765**, 154

Drimmel, R., Cabrera-Lavers, A., and López-Corredoira, M.: 2003, *AA* **409**, 205

Duffau, S., Zinn, R., Vivas, A. K., Carraro, G., Méndez, R. A., Winnick, R., and Gallart, C.: 2006, *ApJL* **636**, L97

Dwek, E., Arendt, R. G., Hauser, M. G., Kelsall, T., Lisse, C. M., Moseley, S. H., Silverberg, R. F., Sodroski, T. J., and Weiland, J. L.: 1995, *ApJ* **445**, 716

Fardal, M. A., Babul, A., Geehan, J. J., and Guhathakurta, P.: 2006, *MN* **366**, 1012

Förster Schreiber, N. M., Genzel, R., Lehnert, M. D., Bouché, N., Verma, A., Erb, D. K., Shapley, A. E., Steidel, C. C., Davies, R., Lutz, D., Nesvadba, N., Tacconi, L. J., Eisenhauer, F., Abuter, R., Gilbert, A., Gillessen, S., and Sternberg, A.: 2006, *ApJ* **645**, 1062

Freeman, K. and Bland-Hawthorn, J.: 2002, *ARA&A* **40**, 487

Freeman, K., Ness, M., Wylie-de-Boer, E., Athanassoula, E., Bland-Hawthorn, J., Asplund, M., Lewis, G., Yong, D., Lane, R., Kiss, L., and Ibata, R.: 2013, *MN* **428**, 3660

Freudenreich, H. T.: 1998, *ApJ* **492**, 495

Fukugita, M., Hogan, C. J., and Peebles, P. J. E.: 1998, *ApJ* **503**, 518

Gerhard, O. and Martinez-Valpuesta, I.: 2012, *ApJL* **744**, L8

Gilmore, G. and Reid, N.: 1983, *MN* **202**, 1025

Gilmore, G., Wyse, R. F. G., and Kuijken, K.: 1989, *ARA&A* **27**, 555

Girardi, L., Bertelli, G., Bressan, A., Chiosi, C., Groenewegen, M. A. T., Marigo, P., Salasnich, B., and Weiss, A.: 2002, *AA* **391**, 195

Girardi, L., Groenewegen, M. A. T., Hatziminaoglou, E., and da Costa, L.: 2005, *AA* **436**, 895

Gonzalez, O. A., Rejkuba, M., Minniti, D., Zoccali, M., Valenti, E., and Saito, R. K.: 2011, *AA* **534**, L14

Gonzalez, O. A., Rejkuba, M., Zoccali, M., Valent, E., Minniti, D., and Tobar, R.: 2013, *AA* **552**, A110

Gonzalez, O. A., Rejkuba, M., Zoccali, M., Valenti, E., Minniti, D., Schultheis, M., Tobar, R., and Chen, B.: 2012, *AA* **543**, A13

Gunn, J. E., Siegmund, W. A., Mannery, E. J., Owen, R. E., Hull, C. L., Leger, R. F., Carey, L. N., Knapp, G. R., York, D. G., Boroski, W. N., Kent, S. M., Lupton, R. H., Rockosi, C. M., Evans, M. L., Waddell, P., Anderson, J. E., Annis, J., Barentine, J. C., Bartoszek, L. M., Bastian, S., Bracker, S. B., Brewington, H. J., Briegel, C. I., Brinkmann, J., Brown, Y. J., Carr, M. A., Czarapata, P. C., Drennan, C. C., Dombeck, T., Federwitz, G. R., Gillespie, B. A., Gonzales, C., Hansen, S. U., Harvanek, M., Hayes, J., Jordan, W., Kinney, E., Klaene, M., Kleinman, S. J., Kron, R. G., Kresinski, J., Lee, G., Limmongkol, S., Lindenmeyer, C. W., Long, D. C., Loomis, C. L., McGehee, P. M., Mantsch, P. M., Neilsen, Jr., E. H., Neswold, R. M., Newman, P. R., Nitta, A., Peoples, Jr., J., Pier, J. R., Prieto, P. S., Prosapio, A., Rivetta, C., Schneider, D. P., Snedden, S., and Wang, S.-i.: 2006, *AJ* **131**, 2332

Harris, W. E.: 1996, *AJ* **112**, 1487

Harris, W. E.: 2010, *ArXiv e-prints*

Helmi, A., Springel, V., and White, S. D. M.: 2002, in G. S. Da Costa, E. M. Sadler, and H. Jerjen (eds.), *The Dynamics, Structure History of Galaxies: A Workshop in Honour of Professor Ken Freeman*, Vol. 273 of *Astronomical Society of the Pacific Conference Series*, p. 333

Helmi, A., White, S. D. M., de Zeeuw, P. T., and Zhao, H.: 1999, *Nat* **402**, 53

Helmi, A., White, S. D. M., and Springel, V.: 2003, *MN* **339**, 834

Hendel, D. and Johnston, K. V.: 2015, *MN* **454**, 2472

Hill, V., Lecureur, A., Gómez, A., Zoccali, M., Schultheis, M., Babusiaux, C., Royer, F., Barbuy, B., Arenou, F., Minniti, D., and Ortolani, S.: 2011, *AA* **534**, A80

Ibata, R. A., Gilmore, G., and Irwin, M. J.: 1994, *Nat* **370**, 194

Jester, S., Schneider, D. P., Richards, G. T., Green, R. F., Schmidt, M., Hall, P. B., Strauss, M. A., Vanden Berk, D. E., Stoughton, C., Gunn, J. E., Brinkmann, J., Kent, S. M., Smith, J. A., Tucker, D. L., and Yanny, B.: 2005, *AJ* **130**, 873

Johnston, K. V., Bullock, J. S., Sharma, S., Font, A., Robertson, B. E., and Leitner, S. N.: 2008, *ApJ* **689**, 936

Jurić, M., Ivezić, Ž., Brooks, A., Lupton, R. H., Schlegel, D., Finkbeiner, D., Padmanabhan, N., Bond, N., Sesar, B., Rockosi, C. M., Knapp, G. R., Gunn, J. E., Sumi, T., Schneider, D. P., Barentine, J. C., Brewington, H. J., Brinkmann, J., Fukugita, M., Harvanek, M., Kleinman, S. J., Krzesinski, J., Long, D., Neilsen, Jr., E. H., Nitta, A., Snedden, S. A., and York, D. G.: 2008a, *ApJ* **673**, 864

Jurić, M., Ivezić, Ž., Brooks, A., Lupton, R. H., Schlegel, D., Finkbeiner, D., Padmanabhan, N., Bond, N., Sesar, B., Rockosi, C. M., Knapp, G. R., Gunn, J. E., Sumi, T., Schneider, D. P., Barentine, J. C., Brewington, H. J., Brinkmann, J., Fukugita, M., Harvanek, M., Kleinman, S. J., Krzesinski, J., Long, D., Neilsen, Jr., E. H., Nitta, A., Snedden, S. A., and York, D. G.: 2008b, *ApJ* **673**, 864

Kapteyn, J. C. and van Rhijn, P. J.: 1920, *ApJ* **52**, 23

Kinman, T. D., Suntzeff, N. B., and Kraft, R. P.: 1994, *AJ* **108**, 1722

Koleva, M., Prugniel, P., Bouchard, A., and Wu, Y.: 2009, *AA* **501**, 1269

Koposov, S. E., Belokurov, V., Evans, N. W., Gilmore, G., Gieles, M., Irwin, M. J., Lewis, G. F., Niederste-Ostholt, M., Peñarrubia, J., Smith, M. C., Bizyaev, D., Malanushenko, E., Malanushenko, V., Schneider, D. P., and Wyse, R. F. G.: 2012, *ApJ* **750**, 80

Kormendy, J. and Barentine, J. C.: 2010, *ApJL* **715**, L176

Kormendy, J. and Kennicutt, Jr., R. C.: 2004, *ARA&A* **42**, 603

Kroupa, P.: 2001, *MN* **322**, 231

Kunder, A., Koch, A., Rich, R. M., de Propris, R., Howard, C. D., Stubbs, S. A., Johnson, C. I., Shen, J., Wang, Y., Robin, A. C., Kormendy, J., Soto, M., Frinchaboy, P., Reitzel, D. B., Zhao, H., and Origlia, L.: 2012, *AJ* **143**, 57

Laney, C. D., Joner, M. D., and Pietrzyński, G.: 2012, *MN* **419**, 1637

Larsen, J. A., Cabanela, J. E., and Humphreys, R. M.: 2011, *AJ* **141**, 130

Lee, J.-W. and Carney, B. W.: 1999, *AJ* **118**, 1373

Mackey, A. D., Huxor, A. P., Ferguson, A. M. N., Irwin, M. J., Tanvir, N. R., McConnachie, A. W., Ibata, R. A., Chapman, S. C., and Lewis, G. F.: 2010, *ApJL* **717**, L11

Majewski, S. R., Skrutskie, M. F., Weinberg, M. D., and Ostheimer, J. C.: 2003a, *ApJ* **599**, 1082

Majewski, S. R., Skrutskie, M. F., Weinberg, M. D., and Ostheimer, J. C.: 2003b, *ApJ* **599**, 1082

Marshall, D. J., Robin, A. C., Reylé, C., Schultheis, M., and Picaud, S.: 2006, *AA* **453**, 635

Martin, N. F., Ibata, R. A., Bellazzini, M., Irwin, M. J., Lewis, G. F., and Dehnen, W.: 2004, *MN* **348**, 12

Martinez-Valpuesta, I. and Gerhard, O.: 2013, *ApJL* **766**, L3

Martinez-Valpuesta, I., Shlosman, I., and Heller, C.: 2006, *ApJ* **637**, 214

Mateu, C., Vivas, A. K., Downes, J. J., Briceño, C., Zinn, R., and Cruz-Diaz, G.: 2012, *MN* **427**, 3374

McWilliam, A. and Rich, R. M.: 1994, *ApJS* **91**, 749

McWilliam, A. and Zoccali, M.: 2010, *ApJ* **724**, 1491

Miceli, A., Rest, A., Stubbs, C. W., Hawley, S. L., Cook, K. H., Magnier, E. A., Krisciunas, K., Bowell, E., and Koehn, B.: 2008, *ApJ* **678**, 865

Mihos, J. C.: 1995, *ApJL* **438**, L75

Minniti, D., Lucas, P. W., Emerson, J. P., Saito, R. K., Hempel, M., Pietrukowicz, P., Ahumada, A. V., Alonso, M. V., Alonso-Garcia, J., Arias, J. I., Bandyopadhyay, R. M., Barbá, R. H., Barbuy, B., Bedin, L. R., Bica, E., Borissova, J., Bronfman, L., Carraro, G., Catelan, M., Clariá, J. J., Cross, N., de Grijs, R., Dékány, I., Drew, J. E., Fariña, C., Feinstein, C., Fernández Lajús, E., Gamen, R. C., Geisler, D., Gieren, W., Goldman, B., Gonzalez, O. A., Gunthardt, G., Gurovich, S., Hambly, N. C., Irwin, M. J., Ivanov, V. D., Jordán, A., Kerins, E., Kinemuchi, K., Kurtev, R., López-Corredoira, M., Maccarone, T., Masetti, N., Merlo, D., Messineo, M., Mirabel, I. F., Monaco, L., Morelli, L., Padilla, N., Palma, T., Parisi, M. C., Pignata, G., Rejkuba, M., Roman-Lopes, A., Sale, S. E., Schreiber, M. R., Schröder, A. C., Smith, M., , Jr., L. S., Soto, M., Tamura, M., Tappert, C., Thompson, M. A., Toledo, I., Zoccali, M., and Pietrzynski, G.: 2010, *New Astronomy* **15**, 433

Momany, Y., Zaggia, S. R., Bonifacio, P., Piotto, G., De Angeli, F., Bedin, L. R., and Carraro, G.: 2004, *AA* **421**, L29

Munari, U., Sordo, R., Castelli, F., and Zwitter, T.: 2005, *AA* **442**, 1127

Nataf, D. M., Gould, A., Fouqué, P., Gonzalez, O. A., Johnson, J. A., Skowron, J., Udalski, A., Szymański, M. K., Kubiak, M., Pietrzyński, G., Soszyński, I., Ulaczyk, K., Wyrzykowski, Ł., and Poleski, R.: 2013, *ApJ* **769**, 88

Nataf, D. M., Udalski, A., Gould, A., Fouqué, P., and Stanek, K. Z.: 2010, *ApJL* **721**, L28

Ness, M., Debattista, V. P., Bensby, T., Feltzing, S., Roškar, R., Cole, D. R., Johnson, J. A., and Freeman, K.: 2014, *ApJL* **787**, L19

Ness, M., Freeman, K., Athanassoula, E., Wylie-De-Boer, E., Bland-Hawthorn, J., Lewis, G. F., Yong, D., Asplund, M., Lane, R. R., Kiss, L. L., and Ibata, R.: 2012, *ApJ* **756**, 22

Newberg, H. J., Yanny, B., Rockosi, C., Grebel, E. K., Rix, H.-W., Brinkmann, J., Csabai, I., Hennessy, G., Hindsley, R. B., Ibata, R., Ivezić, Z., Lamb, D., Nash, E. T., Odenkirchen, M., Rave, H. A., Schneider, D. P., Smith, J. A., Stolte, A., and York, D. G.: 2002, *ApJ* **569**, 245

Nishiyama, S., Tamura, M., Hatano, H., Kato, D., Tanabé, T., Sugitani, K., and Nagata, T.: 2009, *ApJ* **696**, 1407

Norris, J.: 1987, *ApJL* **314**, L39

Oosterhoff, P. T.: 1939, *The Observatory* **62**, 104

Ortolani, S., Renzini, A., Gilmozzi, R., Marconi, G., Barbuy, B., Bica, E., and Rich, R. M.: 1995, *Nat* **377**, 701

Peñarrubia, J., Martínez-Delgado, D., Rix, H. W., Gómez-Flechoso, M. A., Munn, J., Newberg, H., Bell, E. F., Yanny, B., Zucker, D., and Grebel, E. K.: 2005, *ApJ* **626**, 128

Pietrinferni, A., Cassisi, S., Salaris, M., and Castelli, F.: 2004, *ApJ* **612**, 168

Pietrzyński, G., Gieren, W., and Udalski, A.: 2003, *AJ* **125**, 2494

Portail, M., Wegg, C., Gerhard, O., and Martinez-Valpuesta, I.: 2015, *MN* **448**, 713

Preston, G. W., Shectman, S. A., and Beers, T. C.: 1991, *ApJ* **375**, 121

Quinn, P. J., Hernquist, L., and Fullagar, D. P.: 1993, *ApJ* **403**, 74

Rana, N. C. and Basu, S.: 1992, *AA* **265**, 499

Rich, R. M., Reitzel, D. B., Howard, C. D., and Zhao, H.: 2007, *ApJL* **658**, L29

Robin, A. C., Marshall, D. J., Schultheis, M., and Reylé, C.: 2012, *AA* **538**, A106

Robin, A. C., Reylé, C., Derrière, S., and Picaud, S.: 2003, *AA* **409**, 523

Robin, A. C., Reylé, C., Fliri, J., Czekaj, M., Robert, C. P., and Martins, A. M. M.: 2014, *AA* **569**, A13

Rocha-Pinto, H. J., Majewski, S. R., Skrutskie, M. F., Crane, J. D., and Patterson, R. J.: 2004, *ApJ* **615**, 732

Saito, R. K., Minniti, D., Dias, B., Hempel, M., Rejkuba, M., Alonso-García, J., Barbuy, B., Catelan, M., Emerson, J. P., Gonzalez, O. A., Lucas, P. W., and Zoccali, M.: 2012, *AA* **544**, A147

Salaris, M. and Girardi, L.: 2002, *MN* **337**, 332

Salpeter, E. E.: 1955, *ApJ* **121**, 161

Schaye, J., Crain, R. A., Bower, R. G., Furlong, M., Schaller, M., Theuns, T., Dalla Vecchia, C., Frenk, C. S., McCarthy, I. G., Helly, J. C., Jenkins, A., Rosas-Guevara, Y. M., White, S. D. M., Baes, M., Booth, C. M., Camps, P., Navarro, J. F., Qu, Y., Rahmati, A., Sawala, T., Thomas, P. A., and Trayford, J.: 2015, *MN* **446**, 521

Schlegel, D. J., Finkbeiner, D. P., and Davis, M.: 1998a, *ApJ* **500**, 525

Schlegel, D. J., Finkbeiner, D. P., and Davis, M.: 1998b, *ApJ* **500**, 525

Schultheis, M., Chen, B. Q., Jiang, B. W., Gonzalez, O. A., Enokiya, R., Fukui, Y., Torii, K., Rejkuba, M., and Minniti, D.: 2014a, *AA* **566**, A120

Schultheis, M., Ganesh, S., Simon, G., Omont, A., Alard, C., Borsenberger, J., Copet, E., Epchtein, N., Fouqué, P., and Habing, H.: 1999, *AA* **349**, L69

Schultheis, M., Zasowski, G., Allende Prieto, C., and et al: 2014b, *AJ* **148**, 24

Sesar, B.: 2012, *AJ* **144**, 114

Sesar, B., Ivezić, Ž., Grammer, S. H., Morgan, D. P., Becker, A. C., Jurić, M., De Lee, N., Annis, J., Beers, T. C., Fan, X., Lupton, R. H., Gunn, J. E., Knapp, G. R., Jiang, L., Jester, S., Johnston, D. E., and Lampeitl, H.: 2010, *ApJ* **708**, 717

Sesar, B., Ivezić, Ž., Stuart, J. S., Morgan, D. M., Becker, A. C., Sharma, S., Palaversa, L., Jurić, M., Wozniak, P., and Oluseyi, H.: 2013, *AJ* **146**, 21

Sesar, B., Jurić, M., and Ivezić, Ž.: 2011, *ApJ* **731**, 4

Shapley, H.: 1918, *ApJ* 48

Sharma, S., Bland-Hawthorn, J., Johnston, K. V., and Binney, J.: 2011, *ApJ* **730**, 3

Shen, J., Rich, R. M., Kormendy, J., Howard, C. D., De Propris, R., and Kunder, A.: 2010, *ApJL* **720**, L72

Skrutskie, M. F., Cutri, R. M., Stiening, R., Weinberg, M. D., Schneider, S., Carpenter, J. M., Beichman, C., Capps, R., Chester, T., Elias, J., Huchra, J., Liebert, J., Lonsdale, C., Monet, D. G., Price, S., Seitzer, P., Jarrett, T., Kirkpatrick, J. D., Gizis, J. E., Howard, E., Evans, T., Fowler, J., Fullmer, L., Hurt, R., Light, R., Kopan, E. L., Marsh, K. A., McCallon, H. L., Tam, R., Van Dyk, S., and Wheelock, S.: 2006, *AJ* **131**, 1163

Smith, H. A., Catelan, M., and Clementini, G.: 2009, in J. A. Guzik and P. A. Bradley (eds.), *American Institute of Physics Conference Series*, Vol. 1170 of *American Institute of Physics Conference Series*, pp 179–187

Springel, V., Frenk, C. S., and White, S. D. M.: 2006, *Nat* **440**, 1137

Springel, V., Wang, J., Vogelsberger, M., Ludlow, A., Jenkins, A., Helmi, A., Navarro, J. F., Frenk, C. S., and White, S. D. M.: 2008, *MN* **391**, 1685

Stanek, K. Z., Mateo, M., Udalski, A., Szymanski, M., Kaluzny, J., and Kubiak, M.: 1994, *ApJL* **429**, L73

Stanek, K. Z., Udalski, A., SzymaŃski, M., KałuŻny, J., Kubiak, Z. M., Mateo, M., and KrzemiŃski, W.: 1997, *ApJ* **477**, 163

Sumi, T., Wu, X., Udalski, A., Szymański, M., Kubiak, M., Pietrzyński, G., Soszyński, I., Woźniak, P., Żebruń, K., Szewczyk, O., and Wyrzykowski, Ł.: 2004, *MN* **348**, 1439

van der Kruit, P. C. and Freeman, K. C.: 2011, *ARA&A* **49**, 301

van der Kruit, P. C. and Searle, L.: 1981, *AA* **95**, 105

van Dokkum, P. G.: 2001, *PASP* **113**, 1420

Villalobos, Á. and Helmi, A.: 2009, *MN* **399**, 166

Vivas, A. K. and Zinn, R.: 2006, *AJ* **132**, 714

Watkins, L. L., Evans, N. W., Belokurov, V., Smith, M. C., Hewett, P. C., Bramich, D. M., Gilmore, G. F., Irwin, M. J., Vidrih, S., Wyrzykowski, Ł., and Zucker, D. B.: 2009, *MN* **398**, 1757

Wegg, C. and Gerhard, O.: 2013, *MN* **435**, 1874

Wegg, C., Gerhard, O., and Portail, M.: 2015, *MN* **450**, 4050

Weiland, J. L., Arendt, R. G., Berriman, G. B., Dwek, E., Freudenreich, H. T., Hauser, M. G., Kelsall, T., Lisse, C. M., Mitra, M., Moseley, S. H., Odegard, N. P., Silverberg, R. F., Sodroski, T. J., Spiesman, W. J., and Stemwedel, S. W.: 1994, *ApJL* **425**, L81

White, S. D. M. and Rees, M. J.: 1978, *MN* **183**, 341

Xue, X.-X., Ma, Z., Rix, H.-W., Morrison, H. L., Harding, P., Beers, T. C., Ivans, I. I., Jacobson, H. R., Johnson, J., Lee, Y. S., Lucatello, S., Rockosi, C. M., Sobeck, J. S., Yanny, B., Zhao, G., and Allende Prieto, C.: 2014, *ApJ* **784**, 170

Xue, X.-X., Rix, H.-W., Yanny, B., Beers, T. C., Bell, E. F., Zhao, G., Bullock, J. S., Johnston, K. V., Morrison, H., Rockosi, C., Koposov, S. E., Kang, X., Liu, C., Luo, A., Lee, Y. S., and Weaver, B. A.: 2011, *ApJ* **738**, 79

Zinn, R., Horowitz, B., Vivas, A. K., Baltay, C., Ellman, N., Hadjiyska, E., Rabinowitz, D., and Miller, L.: 2014, *ApJ* **781**, 22

Zoccali, M., Hill, V., Lecureur, A., Barbuy, B., Renzini, A., Minniti, D., Gómez, A., and Ortolani, S.: 2008, *AA* **486**, 177

Zorotovic, M., Catelan, M., Smith, H. A., Pritzl, B. J., Aguirre, P., Angulo, R. E., Aravena, M., Assef, R. J., Contreras, C., Cortés, C., De Martini, G., Escobar, M. E., González, D., Jofré, P., Lacerna, I., Navarro, C., Palma, O., Prieto, G. E., Recabarren, E., Triviño, J., and Vidal, E.: 2010, *AJ* **139**, 357